Excited electron correlations in resonant multiphoton ionization via barium Rydberg states

G. Leuchs and S. J. Smith*
Joint Institute for Laboratory Astrophysics, University of Colorado and National Bureau of Standards, Boulder, Colorado 80309
(Received 26 June 1984)

Photoelectron angular distributions have been studied in resonant multiphoton ionization of barium via $J=0$ states, in the region where the $6sns\ ^1S_0$ Rydberg series interacts strongly with the $5d7d\ ^3P_0$ doubly excited state. This interaction is dominantly quadrupole and is localized around $n=18$. The data analysis reveals spin-orbit coupling and strong channel mixing in the continuum.

I. INTRODUCTION

Interest in helium and other two-valence-electron systems, and in characterizing the interactions between different electron configurations induced by the mutual electrostatic repulsion of these electrons, has been accelerated in recent years by the development of the multichannel quantum-defect theory (MQDT) on the one hand, and by new spectroscopic capabilities opened up by laser technology on the other. The status of the theoretical approach to excited-state dynamics has been reviewed recently by Fano,[1] and by Seaton.[2] An overview of applications of MQDT to experimental data on alkaline-earth atoms has been given by Aymar,[3] with the conclusion that term energies alone are not sufficient to provide complete descriptions of these interactions in the MQDT framework. Measurements of other physical parameters are required. We demonstrate, through measurements on the $6sns$, $J=0$ series in atomic barium, that photoelectron angular distribution measurements provide information not otherwise available from other measurements published so far. A particularly interesting property of our present results is that they isolate effects due to a pure quadrupole interaction.

Alkaline-earth atoms have the special property that the $n'sns\ ^1S_0$ singly excited Rydberg series is perturbed by nearby members of a series of levels in which both electrons are promoted. In the case presented here we study the perturbation of the $6sns\ ^1S_0$ series of barium due to the $5d7d\ ^3P_0$ state, which lies near the $6s18s$ state.

In general, the Slater integrals used to determine term energies already contain higher moments of the multipole expansion of the electrostatic interaction $\sim 1/r_{12}$. (In an sd configuration, for example, the electrostatic quadrupole interaction already appears in the exchange integral.) In this respect, $n'sns$ configurations in two-electron atoms are, however, unique since the independent-particle electronic wave functions are spherically symmetrical and, in first-order perturbation theory, the quadrupole contribution to the energy vanishes (as do all other multipole contributions). In barium the perturbation of $6sns$ by the doubly excited $5d7d$ state, however, is a pure quadrupole interaction. The experimental observations are thereby a direct probe of this quadrupole interaction.

After the presentation of the experimental setup and results in Secs. II and III, the theoretical shape of photoelectron angular distributions and in particular its dependence on the mixture between the two interacting channels is discussed in Sec. IV. In Sec. V the experimental data are reduced to give ionization amplitudes and channel admixture coefficients. The signs of the latter are obtained in dependence on the phases of the bound-free matrix elements. Finally, it is shown that the channel admixture coefficients obtained here correctly predict the line strength in the $6s6p \rightarrow 6sns$ absorption spectra.

II. EXPERIMENTAL SETUP

We have measured the angular distributions of photoelectrons produced in a field-free region from $6sns\ ^1S_0$ excited states of atomic barium, for $15 \leq n \leq 20$, in a plane transverse to the direction of propagation of linearly polarized 1.06 μm [Nd:YAG (yttrium aluminum garnet) pulsed laser] ionizing radiation. Photoelectrons emitted into a 12° half-angle cone along a fixed axis were detected by a 16-stage secondary-emission multiplier. With the detection rate R in the range $\lesssim 0.3$ photoelectron counts per laser pulse, we measured this rate as the polarization vector was rotated by 10° increments in the transverse plane using a $\lambda/2$ retarding plate. These rates were normalized to measured total photoion production per pulse, and corrected for two- and more-electron events using experimentally verified Poisson statistics for the photoelectron counts. The maximum correction applied was 15%. The measurement was carried out in a high-vacuum atomic-beam apparatus using a barium atom density of $\sim 10^6$ atoms/cm^3 in a $\sim$1-mm-diam beam with $\sim$5 milliradian divergence.

The $6sns$ atoms were prepared by resonant excitation through the $6s6p\ ^1P_1$ level using synchronously pumped linearly polarized dye-laser pulses, superposed in time and space, with the polarization controlled by a common Glan-Thompson prism and a common $\lambda/2$ achromatic retarding plate. These $\sim$6 ns pulses at 553.7 and $\sim$420 nm preceded the $\sim$9 ns ionizing pulse by $\sim$15 ns, a time short compared to lifetimes of the $6sns\ ^1S_0$ states of interest (Aymar *et al.*[4]). The common propagation axis of these laser pulses was at an angle of 1.7° to that of the 1.06 μm ionizing radiation, to permit use of a separate 1.06-μm $\lambda/2$ retarding plate. The $6s^2\ ^1S_0 - 6s6p\ ^1P_1$ transition was saturated by $\sim$100 W peak power 553.7 nm pulses. The second laser intensity was controlled ($\sim$kW

peak power) to minimize power broadening. The region of the continuum into which the atoms are ionized is structureless.[5] The energy of the ionizing photons is higher than the threshold of the $5d\epsilon l$-continuum so that the final state of the barium ion may be $6s\,^2S_{1/2}$, $5d\,^2D_{3/2}$, or $5d\,^2D_{5/2}$. We used time-of-flight discrimination to detect only those photoelectrons which leave the barium ion in the $6s\,^2S_{1/2}$ ground state.

One critical requirement on the optics was the effective elimination of displacement and deviation of laser beams by rotating optical components. This was accomplished by careful alignment and by insertion of crossed wedges to compensate for the wedge in the $\lambda/2$ plates. Another critical requirement is on the polarization axes of the three lasers, which must remain synchronized (parallel) at all angles of rotation. They were set by minimizing transmission of each through a reference Glan prism, using a sensitive photodiode. This also tested the quality of linear polarization. Transverse components are $\lesssim 10^{-2}$ of the radiation intensity.

Laser beam waists were ~ 200—$400\,\mu$m in diameter, defining a reaction volume containing $\sim 10^2$—10^3 barium atoms. The collection efficiency was $\sim 10^{-2}$. The 1.06 μm pulses (~ 150 mJ per pulse) were sufficient to saturate or nearly saturate the photoionization process. The rate R was controlled by neutral density filters in the second laser beam (control of excited atom density) or by limiting YAG pulse power.

III. RESULTS

Photoelectron angular distributions in N-photon ionization are of the general form[6,7]

$$I_N(\theta) \propto 1 + \sum_{k=1}^{N} \beta_{2k} P_{2k}(\cos\theta) \,, \tag{1}$$

where θ is the angle between electron emission and the direction of linear laser polarization. For the $J=0$ states studied here, the ionizing radiation couples only to the $J=1$ continuum, and transition matrix elements contain angular dependences no higher than $\cos^2\theta$. Therefore, photoelectron angular distributions must be of the form $I_1(\theta)$.

The $6sns$ resonances, observed in a photoionization spectrum, appear as very small but well resolved peaks interspersed between members of the much stronger $6snd$ series. Figure 1 shows two ionization spectra taken at two different intensities of the dye laser exciting the $6s\,6p\,{}^1P_1$ to $6snl$ transitions. Figure 1(a) was taken with $\theta=0°$ and with low-laser intensity to minimize broadening. For the higher-intensity laser spectrum [Fig. 1(b)] the angle θ was adjusted to 45° because it minimizes the spurious photoelectron background which arises from a spectrally broad continuum in the dye-laser beam, from spontaneous emission amplified in the high-gain dye medium.

The intensity of the broad continuum varies according to what part of the dye-gain curve is being used for the primary laser action; it is small at the center and increases as the central dye-laser frequency moves toward the ends of the gain curve. When the laser is operated at the fairly high-power levels necessary to generate sizable $6sns$ state

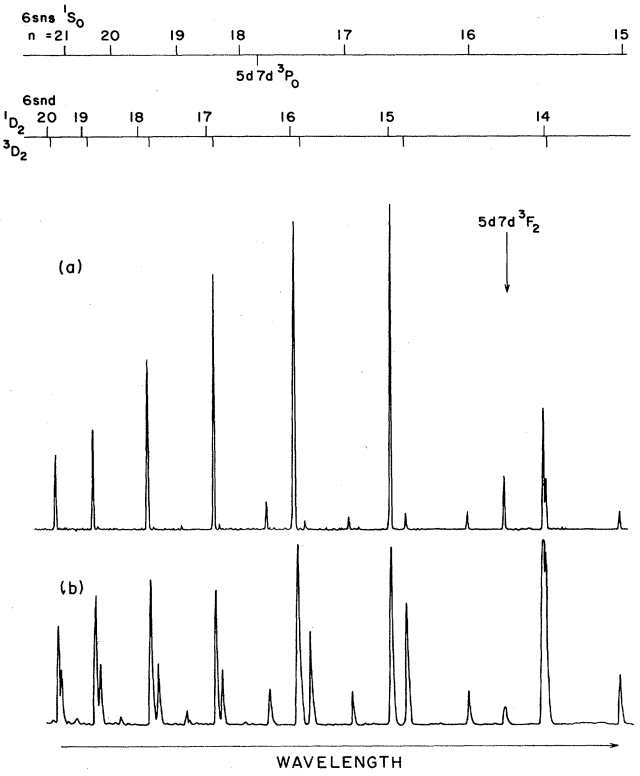

FIG. 1. Resonant three-photon ionization spectra of barium via $6sns\ {}^1S_0$ states in the range from $n=15$ to 21, for two different laser intensities: (a) $\theta=0°$, $I\cong 10^6$ W/cm^2, (b) $\theta=45°$, $I\cong 10^8$ W/cm^2. Saturation effects are obvious in linewidth and intensity ratios. Note that spectrum (b) was recorded with a lower detector sensitivity than (a).

populations [as in Fig. 1(b)], the broadband background may induce transitions having high oscillator strengths, such as the ones to the $6snd$ states. As a result the ionizing (YAG 1.06 μm) radiation ionizes not only from the $6sns$ state to which the dye laser is tuned, but also from a range of $6snd$ states excited by the fluorescence background, which introduces P_4 and P_6 components to the angular distribution.[8,9] Polar plots of the measured angular distributions are shown in Fig. 2 with the best fit of $I_3(\theta)$ represented in the solid curve. In all cases shown, the background induced values of β_4 and β_6 were less than 0.05 and 0.04, respectively.

Corrections to the $6sns$ angular distributions were derived from off-line measurements of background photoelectron angular distributions. The corrections were scaled to minimize the content of even Legendre polynomials higher than P_2. The values of β_2 obtained after correcting for the background are plotted in Fig. 3. In the region of n studied here the state designated as $5d\,7d\,{}^3P_0$ is the $J=0$ state with the shortest lifetime,[4] the smallest diamagnetic shift,[10] the largest admixture of the pure $5d\,7d$ configuration[11] and the largest isotope shift.[12] In contrast to this, the photoelectron angular distribution is extreme for the $6s\,18s\ {}^1S_0$ and not for the $5d\,7d\ {}^3P_0$ state.

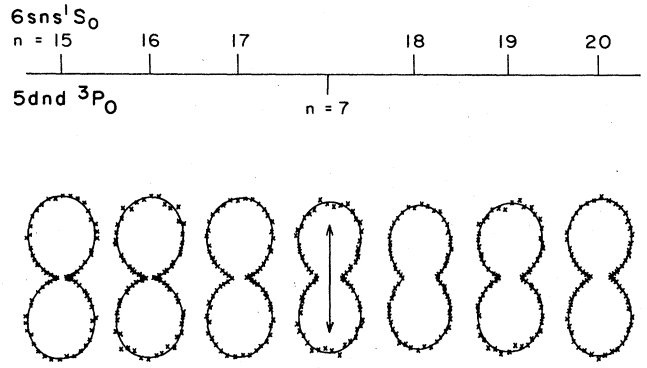

FIG. 2. Polar diagrams of photoelectron angular distributions in three-photon ionization of barium via high-lying $J=0$ intermediate states. The arrow indicates the linear polarization direction of the laser radiation. The solid line represents the least-squares fit of $I_3(\theta)$ to the data (crosses).

This surprising result is due to interferences between different ionization channels. It exemplifies that angular distributions yield information about the relative signs of state admixture coefficients and ionization amplitudes unlike all the other measurements listed above which are sensitive only to the squares of these admixture coefficients. Another manifestation of interference occurs in the ionization spectrum (Fig. 1). Ionization via the $6s\,18s\ ^1S_0$ and via the $5d\,7d\ ^3P_0$ states leads to drastically different signal intensities.

The solid line in Fig. 3 represents the result of a least-squares fit of a Fano profile[13]

$$\beta_2(E)=a-\frac{[b+c(E-E_0)]^2}{\Gamma^2/4+(E-E_0)^2} \tag{2}$$

to the experimental data. The use of a Fano profile is suggested whenever there is a bound state embedded in a continuum. Although no continuum is involved here, there is a dense series of $6sns$ states. The parameter values for the curve shown in Fig. 3 are $E_0=41\,464.5\pm9.9$ cm^{-1}, $\Gamma^2/4=4126\pm800$ cm^{-2}, $a=1.758\pm0.027$, $b=52.8\pm5.9$ cm^{-1}, and $c=0.075\pm0.042$. The error bars correspond to single standard deviations. As a result of the large error bar for c, the Fano q parameter, $q=2b/(c\Gamma)=11$ has a similar uncertainty. The asymptotic value for $\beta_2(E)$ in the limit of large $E-E_0$ is $\beta_2=a-c^2=1.753\pm0.030$. The deviation of $\beta_2(E-E_0\gg\Gamma)$ from two indicates the importance of spin-orbit coupling.[14]

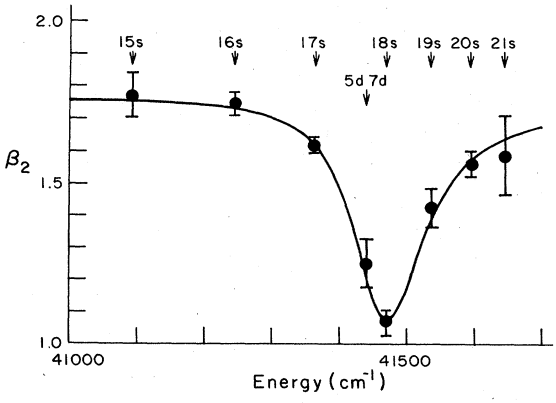

FIG. 3. Experimentally determined photoelectron angular distribution parameters β_2 plotted vs the energy of the second resonant intermediate state in three-photon ionization of barium. The error bars represent the scatter of β_2 for different experimental runs. The solid line was fitted using a Fano profile.

IV. THEORETICAL DESCRIPTION

The theory of atomic photoionization has recently been reviewed by Starace.[14] He discussed the dipolar electron angular distributions which occur in one-photon ionization from spatially isotropic states where all m substates are equally populated. Multiphoton absorption into the continuum in general introduces multipole anisotropy to the angular distribution which is higher than dipole.[6] This, however, does not hold if the intermediate state is $J=0$, i.e., spherically symmetrical, the case of interest in this paper.

A. Intermediate bound states

The $J=0$ states studied here belong to Rydberg series converging to the Ba II $6s\ ^2S_{1/2}$, $5d\ ^2D_{3/2}$, and $5d\ ^2D_{5/2}$ limits. Therefore, it seems appropriate to use a three-channel model to describe the highly excited $J=0$ states. In their MQDT analysis of the term energies of the even parity $J=0$ states between $6s\,8s$ and $6s\,45s$ Aymar *et al.*[11] have also allowed for a fourth channel converging to the Ba II ^2P limit. In the region around $n=18$, however, they found that the excited states can be well represented by superpositions of three channels

$$|\psi\rangle=Z_{\bar{1}}\,|\,6sns\ ^1S_0\rangle+Z_{\bar{2}}\,|\,5dn'd\ ^3P_0\rangle+Z_{\bar{3}}\,|\,5dn'd\ ^1S_0\rangle\ . \tag{3}$$

Here the excited-state wave function $|\psi\rangle$ is expanded in three LS-coupled channels. The corresponding collisional channel basis is $6s[^2S_{1/2}]ns_{1/2}$, $5d[^2D_{3/2}]n'd_{3/2}$, and $5d[^2D_{5/2}]n'd_{5/2}$. According to Aymar *et al.*,[11] the dominant admixture coefficients around $n=18$ are $Z_{\bar{1}}^2$ and $Z_{\bar{2}}^2$, with $Z_{\bar{3}}^2$ being at most about 8% of $(Z_{\bar{1}}^2+Z_{\bar{2}}^2)$. We note also that the energy difference between the two $5d$ limits is only 14% of the energy separation between the levels under study and the $5d$ limits. Therefore, we decided to try the two-channel model

$$|\psi\rangle=Z_1\,|\,6sns\ ^1S_0\rangle^0+Z_2\,|\,5dn'd\ ,J=0\rangle^0\ . \tag{4}$$

$Z_1=Z_{\bar{1}}$ and $|Z_2|=(Z_{\bar{2}}^2+Z_{\bar{3}}^2)^{1/2}=(1-Z_{\bar{1}}^2)^{1/2}$ are the coefficients in the collisional channel basis and the superscript "0" indicates a pure configuration state. The two-channel model simplifies the analysis also since it reduces the number of photoionization channels, and proves to be quite useful for the interpretation of our data.

B. Continuum

The final continuum states in the three-photon-ionization process studied here must have a total angular momentum of $J=1$. The magnetic quantum number is $M_J=0$, since all three lasers have the same direction of linear polarization. Time-of-flight discrimination of slow photoelectrons ensures that only ionization into the $6s\epsilon l$ continuum is observed in the experiment. Therefore, there are four possible final states:

$$|6s_{1/2},m_s;\epsilon p_j,m_j;J=1\rangle$$

with $j=\frac{1}{2}$, $\frac{3}{2}$, and $m_s,m_j=\pm\frac{1}{2}$, $M_J=m_s+m_j=0$. Interferences are observed only between continuum states having identical ion core quantum numbers. Since, owing to the symmetry of the problem, ionization into the $6s,m_s=\frac{1}{2}$, and $6s,m_s=-\frac{1}{2}$ final states of the ion leads to the same angular distribution of photoelectrons, only the case $6s,m_s=-\frac{1}{2}$ will be considered here. The electron angular distribution is then given by

$$\frac{d\sigma}{d\Omega}\sim\sum_{\substack{\text{spin}\\ \text{states}}}|(Z_1s_1+Z_2d_1)X_{1/2}(\theta,\phi) -\sqrt{2}(Z_1s_3+Z_2d_3)X_{3/2}(\theta,\phi)|^2 ,$$

$$X_{1/2}(\theta,\phi)=\sqrt{1/3}Y_{10}(\theta,\phi)\psi_+ +\sqrt{2/3}Y_{11}(\theta,\phi)\psi_- ,$$
$$X_{3/2}(\theta,\phi)=\sqrt{2/3}Y_{10}(\theta,\phi)\psi_+ +\sqrt{1/3}Y_{11}(\theta,\phi)\psi_- . \quad (5)$$

The spherical angles θ and ϕ describe the direction of the electron wave vector $\mathbf{k}$ relative to the direction of light polarization. The electron spin is not measured in this experiment. Therefore, the differential cross section has to be summed over both spin states ψ_+ and ψ_-. Consequently, cross terms between different spin states vanish. The ionization amplitudes from the pure-configuration bound states $|6sns\ ^1S_0\rangle^0$ and $|5d7d,J=0\rangle^0$ into the $|\epsilon p_{1/2}\rangle$ and $|\epsilon p_{3/2}\rangle$ continuum states are represented by $s_1(n)$, d_1, $-\sqrt{2}s_3(n)$, and $-\sqrt{2}d_3$ which are designated as shown in Fig. 4. The factor "$-\sqrt{2}$" comes from the angular integration and the amplitudes $s_1(n)$, $s_3(n)$, d_1, and d_3 are the radial matrix elements. If the $|\epsilon p_j\rangle$ continuum states belong to the pure $6s\epsilon p$ configuration, then d_1 and d_3 are both zero. Therefore, experimentally determined nonzero values for d_1 and d_3 will indicate channel mixing in the continuum. Since the cross section for photoionization out of excited-states scales as $(n-\mu)^{-3}$, μ being the quantum defect, $|s_1|$ and $|s_3|$ are proportional to $(n-\mu)^{-3/2}$.

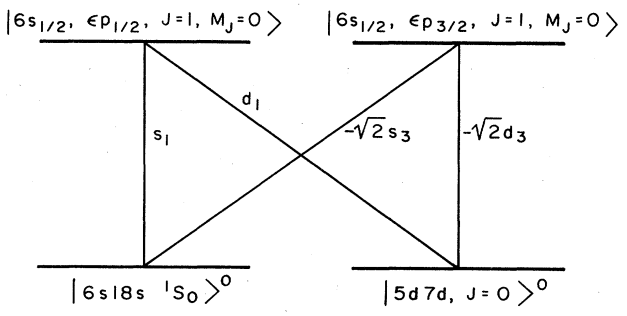

FIG. 4. Ionization amplitudes for transitions from $J=0$ pure configuration bound to continuum states.

For the analysis of our data, Eq. (5) has been evaluated to give the anisotropy parameter β_2 of Eq. (1) as a function of the state admixture coefficients Z_1 and Z_2 and of the ionization amplitudes:

$$\beta_2=\frac{Z_1^2(2|s_3|^2+4\mathrm{Re}\{s_1s_3^*\})+4Z_1Z_2\mathrm{Re}\{s_3d_3^*+s_1d_3^*+s_3d_1^*\}+Z_2^2(2|d_3|^2+4\mathrm{Re}\{d_1d_3^*\})}{Z_1^2(|s_1|^2+2|s_3|^2)+Z_2^2(|d_1|^2+2|d_3|^2)+2Z_1Z_2\mathrm{Re}\{s_1d_1^*+2s_3d_3^*\}} , \quad (6)$$

for a given n. The denominator is proportional to the angle integrated cross section. In the case $Z_2=0$, Eq. (6) reduces to Eq. (23.7b) of Starace.[14]

V. EVALUATION OF THE RESULTS

The number of parameters appearing in Eq. (6) is greater than the number of anisotropy parameters $\beta_2(n)$ determined experimentally. We have, therefore, used the results of the MQDT analysis of level positions by Aymar *et al.*[11] to extract Z_2^2. For the levels $n=15$, 16, 20, and 21, Aymar *et al.*[11] do not give numbers for the Z_2^2 explicitly, so we determined Z_2^2 graphically from a Lu-Fano plot (Fig. 1 of Ref. 15 and Fig. 4 of Ref. 11) using the formula[15]

$$Z_2^2=-(\nu_d^3\,d\nu_s/d\nu_d)(\nu_s^3-\nu_d^3\,d\nu_s/d\nu_d)^{-1} , \quad (7)$$

where ν_s and ν_d are the effective quantum numbers evaluated with respect to the $6s$ and the $5d$ limit, respectively. The dependence of the angular distribution anisotropy parameter on Z_2 is given by Eq. (6). For the purpose of analyzing the data we have included the scaling factor $|f(n)|=[(18-\mu)/(n-\mu)]^{3/2}$, $\mu=4.2$, so that $|s_i(n)|=|f(n)s_i(n=18)|$, $i=1,3$. These measures reduced the number of independent parameters to six, which as it turned out is still too large to give a stable least-squares fit of Eq. (6) to the data.

The six parameters are the absolute values and complex phases of the relative ionization amplitudes s_3/s_1, d_1/s_1, and d_3/s_1. The complex phases originate from the complex nature of the continuum wave function, where deviations from a hydrogenic wave function manifest themselves in the scattering phase[6,14] δ_j, which can be extrapolated from the quantum defect μ_j of the corresponding

bound states,[2] $\delta_j=\pi\mu_j$. For the barium $6snp_j$ Rydberg series the quantum defects have been determined by Armstrong *et al.*[16] yielding $\cos(\delta_{1/2}-\delta_{3/2})\simeq 0.997$ at the ionization threshold. Furthermore, the quantum-defect difference is only weakly energy dependent. Since for ionization with ~ 1.1-eV Nd:YAG laser photons a structureless region of the continuum is reached,[5] this extrapolation is expected to be fairly good. We have, therefore, assumed $\cos(\delta_{1/2}-\delta_{3/2})=1$, and, consequently, take $\mathrm{Re}\{s_1 s_3^*\}=|s_1 s_3|$ and likewise $\mathrm{Re}\{d_1 d_3^*\}=|d_1 d_3|$.

We note in passing that a similar phase-shift difference has been calculated for the $\epsilon p_{1/2}$ and $\epsilon p_{3/2}$ partial waves of cesium by Huang and Starace.[17] The similarity between barium and cesium, as far as spin-orbit effects in the continuum are concerned, is suggested by the proximity of barium to cesium in the Periodic Table. Therefore, it is not surprising that Huang and Starace[17] calculate a β_2 for photoionization of ground-state cesium atoms which, for energies larger than the Cooper minimum, asymptotically approaches a value ($\beta_2\approx 1.8$), which is very close to the value of β_2 we observed for barium in the limit of $E-E_0\gg\Gamma$, far away from the $5d7d$ perturber [see Eq. (2)].

With the above assumptions we reduced the number of fitting parameters to four, $|s_3/s_1|$, $|d_1/s_1|$, $|d_3/s_1|$, and δ_{sd}, the phase difference of the s_i and d_i ionization amplitudes. The modification of Eq. (6) finally used in the least-squares fitting routine was

$$\beta_2(n)=\frac{A[f(n)]^2[Z_1(n)]^2+Bf(n)Z_1(n)Z_2(n)+C[Z_2(n)]^2}{D[f(n)]^2[Z_1(n)]^2+Ef(n)Z_1(n)Z_2(n)+F[Z_2(n)]^2} \tag{8}$$

with

$$A=2|s_3|^2+4|s_1 s_3|\ ,$$

$$B=4(|s_3 d_3|+|s_1 d_3|+|s_3 d_1|)\cos\delta_{sd}\ ,$$

$$C=2|d_3|^2+4|d_1 d_3|\ ,$$

$$D=|s_1|^2+2|s_3|^2\ ,$$

$$E=2(|s_1 d_1|+2|d_3 s_3|)\cos\delta_{sd}\ ,$$

and

$$F=|d_1|^2+2|d_3|^2\ .$$

Equation (8) also holds for the $|5d7d,J=0\rangle$ state. In this case $f(n)$ has to be set equal to $f(18)=1$ since the Rydberg character of the $|5d7d,J=0\rangle$ state is mainly that of the $|6s18s\ ^1S_0\rangle$ state (see discussion below). One ambiguity that remained is the sign of the interference term $f(n)Z_1(n)Z_2(n)\cos\delta_{sd}$, which cannot be deduced from any of the measurements on the barium $6sns\ ^1S_0$ Rydberg series published previously.[3,4,10–12,18] We, therefore, repeated the least-squares fit of Eq. (8) to the data for various sets of sign combinations. By far the best model was to have a positive sign for $n=15$ to $n=17$ and the $5d7d$ perturber, and to have a negative sign for $n=18$ to $n=21$. The numbers for $[f(n)]^2[Z_1(n)]^2$, $[Z_2(n)]^2$, and $f(n)Z_1(n)Z_2(n)$ used in the final least-squares fit are listed in Table I. Flipping all signs of $f(n)Z_1(n)Z_2(n)$ results in the same fit if the sign of $\cos\delta_{sd}$ is also flipped. Owing to the quadratic dependence of $A,\ldots,F$ in Eq. (8) on the ionization amplitudes we found two different sets of parameters fitting the data equally well (Table II).

Again, we stress the similarity between cesium and barium to pick the physically most meaningful set of ionization amplitudes. Owing to interference between the bound and continuum wave functions the electric dipole transition matrix element goes through zero for a certain photoelectron energy.[19] The effect of spin-orbit coupling and other core interactions is to shrink the $\epsilon p_{1/2}$ wave function more than the $\epsilon p_{3/2}$ so that the ionization amplitude s_1 goes through zero at a lower energy than s_3.[20] For Cs the corresponding drastic change in the photoelectron angular distribution anisotropy parameter β_2 has been calculated by Huang and Starace.[17] Owing to the negligibly small phase-shift difference already mentioned above, β_2 can, in the case of cesium, be written as

$$\beta_2=2(|s_3|^2+2|s_1 s_3|)/(|s_1|^2+2|s_3|^2)\ .$$

It is obvious that one obtains $\beta_2=2$ only for $|s_1|=|s_3|$. But since, according to Huang and Starace,[17] $\beta_2<2$ even in the limit of high energies, $|s_3|$ will be smaller than $|s_1|$ in the whole range above the energy where $|s_3|=0$. A related effect has been observed in photoionization of atoms, where the branching ratio for ionization into different fine-structure states of the ion was found to deviate from the statistical ratio in a way to amplify the lower j partial cross section.[21]

Therefore, we think that, also for barium, the right set of parameters is set A, the one with $|s_3|<|s_1|$. This choice is supported by the fact that the mixing between

TABLE I. List of coefficients used in the least-squares fit of Eq. (8) to β_2^{expt}. The parameters β_2^{fit} computed from Eq. (8) using the best fit ionization amplitudes given in Table II are also shown.

Level energy (cm^{-1})	Assignment	fZ_1Z_2	Z_2^2	$f^2Z_1^2$	β_2^{expt}	β_2^{fit}
41 093	$6s\,15s\ ^1S_0$	0.101	0.005	2.075	1.772±0.066	1.772
41 245	$6s\,16s\ ^1S_0$	0.125	0.010	1.585	1.744±0.033	1.734
41 362	$6s\,17s\ ^1S_0$	0.174	0.025	1.219	1.615±0.018	1.620
41 441	$5d\,7d\ ^3P_0$	0.476	0.653	0.347	1.252±0.073	1.169
41 468	$6s\,18s\ ^1S_0$	−0.452	0.285	0.716	1.065±0.039	1.087
41 535	$6s\,19s\ ^1S_0$	−0.115	0.017	0.796	1.425±0.059	1.393
41 596	$6s\,20s\ ^1S_0$	−0.058	0.005	0.663	1.561±0.039	1.564
41 646	$6s\,21s\ ^1S_0$	−0.041	0.003	0.552	1.584±0.025	1.605

TABLE II. Ionization amplitudes resulting from the least-squares fit of Eq. (8) to the angular distribution data. Two parameter sets fit the data equally well. Note that $\cos\delta_{sd}$ is the same in both sets. Based on comparison with other atoms (see text), set B can be ruled out.

	Parameter set A	B
$\lvert s_3/s_1\rvert$	0.571±0.015	1.99 ±0.02
$\lvert d_1/s_1\rvert$	0.38 ±0.09	15.4 ±1.5
$\lvert d_3/s_1\rvert$	5.04 ±0.50	4.4 ±0.5
$\cos\delta_{sd}$	0.149±0.018	0.149±0.018

the $5dnl$ and $6snp_{3/2}$ channels is larger than the one between the $5dnl$ and $6snp_{1/2}$ channels.[16] In agreement with this, set A gives $\lvert d_3\rvert \gg \lvert d_1\rvert$. It is interesting to note that the transition amplitude d_3 from the $\lvert 5d\,7d\rangle^0$ bound state to the $\lvert 6s\epsilon p_{3/2}\rangle$ continuum state is considerably larger than the amplitude s_3 from $\lvert 6s\,18s\rangle^0$ to $\lvert 6s\epsilon p_{3/2}\rangle$. Since d_3 and d_1 should be zero in the absence of final-state configuration interaction, the large value for d_3 underlines the importance of channel mixing between the different continua of barium.

VI. DISCUSSION

In the last section we have given a set of ionization amplitudes which reproduce the angular distribution data. The picture is still incomplete, though, since the line intensities in the ionization spectrum are yet to be explained. The optimum set of signs for $f(n)Z_1(n)Z_2(n)$, found in the least-squares fit is uncertain by an overall factor ±1, an issue which cannot be resolved based on the experimental data alone.

For the photoionization spectrum shown in Fig. 1 the most intense ionization line via a $J=0$ state is the one via the $5d\,7d$, $J=0$ perturber. This is expected because the ionization amplitude d_3 is far larger than s_1 and s_3. A somewhat surprising feature, however, is the low intensity for the $6s\,18s\ ^1S_0$ intermediate state, which seems to contradict the large amount of the $5d\,7d$ configuration known to be admixed to this state. A first thought is that the ionization amplitudes Z_1s_i and Z_2d_i may cancel each other if Z_2 and Z_1 in Eq. (4) have opposite signs for the $6s\,18s\ ^1S_0$ state. In view of the dominant nature of the d_3 amplitude, however, this explanation has to be abandoned. Therefore, the cancellation must already occur *in the excitation step* from the $6s\,6p$ to the $6s\,18s\ ^1S_0$ state. It should, therefore, be apparent in the photoabsorption measurements of Fonck *et al.*[10] and of Rubbmark *et al.*[22] Unfortunately, neither of these two publications actually shows an absorption spectrum in the region around the $6s\,18s$ state and we had to go back to yet unpublished material by Fonck *et al.*[23] There it was indeed found that the $6s\,18s\ ^1S_0$ state appears as an extremely weak absorption line and that for $n>18$ the line strength was considerably smaller than for $n<18$. This asymmetry between the line intensities has also been observed in the ionization spectrum (Fig. 1). If we denote by a_{ps} and a_{pd} the excitation amplitudes from the real $6s\,6p\ ^1P_1$ to the $\lvert 6s\,18s\ ^1S_0\rangle^0$ and $\lvert 5d\,7d, J=0\rangle^0$ pure configuration states, respectively, then the low absorption strength to the $6s\,18s$ level and the relatively high absorption on the transition to the $5d\,7d$ level means that

$$[a_{ps}Z_1(18)+a_{pd}Z_2(18)]^2\cong 0\ , \tag{9a}$$

and

$$[a_{ps}Z_1(5d\,7d)+a_{pd}Z_2(5d\,7d)]^2=I(5d\,7d)\neq 0\ . \tag{9b}$$

Since the Z_i^2 for these two levels are both of the same order of magnitude the drastic difference in the line intensities can only be explained by opposite signs for the two Z_2's in agreement with the sign change of fZ_1Z_2 found in the analysis of the angular distribution (Table I). Before the admixture coefficients Z_1 and Z_2 can be used to predict the strength of the absorption lines, the signs of $f(n)$, $Z_1(n)$ and of the excitation amplitudes $a_{ps}(n)$ have to be examined.

From the general MQDT formula[24] for the admixture coefficient Z_i it is obvious that the one describing the admixture of the Rydberg series, Z_1, should have a sign alternating with n.[25] The amplitude for transitions between bound states and also for transitions into the continuum show the same sign alternation. The sign of the ionization amplitude in particular is given by the sign of[26]

$$\cos\pi[\nu+\mu(\epsilon)+\chi(\nu l,\epsilon l')]\ .$$

For ionization of Rydberg states the effective principal quantum number ν evaluated with respect to the limit of the Rydberg series is large, the photoelectron kinetic energy ϵ is essentially constant if the wavelength of the ionizing light is not varied, and the phase shift $\pi[\mu(\epsilon)+\chi(\nu l,\epsilon l')]$ is independent of ν.[26] We can, therefore, determine the sign of the n-scaling factor $f(n)$ used, e.g., in Eq. (8),

$$f(n)=(-1)^n[(18-\mu)/(n-\mu)]^{3/2}\ . \tag{10}$$

The alternating sign of Z_1 is correlated with the sign of $f(n)$ to give $Z_1(n)f(n)>0$ independent of n. The sign of $fZ_1Z_2\cos\delta_{sd}$ given in Table I, therefore, directly gives the sign of $Z_2\cos\delta_d$ and therefore the relative sign of Z_2 (see Table III). Where nonresonant channel mixing dominates, the sign of Z_2 may not change along a whole Rydberg series,[25] but if, as in the present case, a local resonant perturbation dominates, Z_2 may change sign.

With these relative signs of Z_1 and Z_2 we can go back to Eqs. (9) and solve them for a_{ps} and a_{pd} in order to

TABLE III. Admixture coefficients Z_1 and Z_2 for the two-channel model.

Level energy (cm^{-1})	Assignment	Z_1	Z_2
41 093	$6s\,15s\ ^1S_0$	−0.998	0.070
41 245	$6s\,16s\ ^1S_0$	0.995	0.099
41 362	$6s\,17s\ ^1S_0$	−0.987	0.158
41 441	$5d\,7d\ ^3P_0$	0.589	0.808
41 468	$6s\,18s\ ^1S_0$	0.846	−0.534
41 535	$6s\,19s\ ^1S_0$	−0.991	−0.129
41 596	$6s\,20s\ ^1S_0$	0.997	−0.071
41 646	$6s\,21s\ ^1S_0$	−0.998	−0.055

predict what the absorption strength of the lower and higher lying $6sns$ states should be. The excitation amplitude a_{ps} has the same n dependence as the ionization amplitude, including the alternating sign [see Eq. (10)]. The absorption line strengths predicted by $A(n)=[f(n)Z_1a_{ps}+Z_2a_{pd}]^2$ and the ones observed by Fonck *et al.*[23] are listed in Table IV and show good agreement. A quantitative evaluation of the ionization spectra in Fig. 1 is complicated by partial saturation of the bound-bound transition, an effect which is different for the different states. The relative ionization signal via the $5d7d$ state in particular is smaller than expected from the large absorption and ionization amplitudes. The $6s18s$ state shows up stronger than in the absorption spectrum since it is amplified by the large ionization amplitude d_3. The same holds for the other $6sns$ states. The strong asymmetry between the $n<18$ and $n>18$ states observed in the absorption spectrum is also apparent in the ionization spectrum.

We have already pointed out that the interaction between the doubly excited perturber and the Rydberg series is rather localized in energy. This suggests, as already remarked by Lu and Rau[15] and by Rinneberg *et al.*,[18] that the interaction between the $6s18s$ and the $5d7d$ state can to a certain extent be described using perturbation theory.

In the following we will estimate the validity of the assumption of localized interaction by analyzing the coupling between the two levels as if they were isolated. Extrapolating the quantum defect μ_s from lower- and higher-lying members of the $6sns$ series[11] one obtains $\mu_s\simeq 4.205$ yielding an unperturbed position of the $6s18s$ state of $E_{18}^{(0)}=41\,458.4$ cm^{-1}. Since the actual level energies are $E_{18}=41\,467.8$ cm^{-1} and $E_{dd}=41\,441.2$ cm^{-1}, the unperturbed position of the $5d7d\,J=0$ state should be located symmetrically at $E_{dd}^{(0)}=41\,450.6$ cm^{-1} (Fig. 5). The interaction energy $|\langle V\rangle|$ has been calculated by diagonalizing the 2×2 energy matrix

$$E_{18,dd}=(E_{18}^{(0)}+E_{dd}^{(0)})/2 \pm[(E_{18}^{(0)}-E_{dd}^{(0)})^2/4+|\langle V\rangle|^2]^{1/2} \quad (11)$$

yielding $|\langle V\rangle|=12.7$ cm^{-1}. The admixture $Z_1^2(5d7d)$ of the $|6s18s\rangle^0$ to the $|5d7d\rangle^0$ state resulting from this diagonalization is $Z_1^2=0.35$, in agreement with the value

TABLE IV. Predicted line intensities in the $6s6p\,^1P_1-6sns\,^1S_0$ absorption spectrum. Experimental data by Fonck *et al.* (Ref. 23) are shown for comparison.

Level energy (cm^{-1})	Assignment	A_{pred}	A_{expt}
41 093	$6s15s\,^1S_0$	6.6	
41 245	$6s16s\,^1S_0$	5.7	
41 362	$6s17s\,^1S_0$	5.3	5.4
41 441	$5d7d\,^3P_0$	10.0[a]	10.0
41 468	$6s18s\,^1S_0$	0.0[a]	0.0
41 535	$6s19s\,^1S_0$	1.3	0.9
41 596	$6s20s\,^1S_0$	1.4	0.7
41 646	$6s21s\,^1S_0$	1.2	0.9

[a]Values adjusted using Eqs. (9).

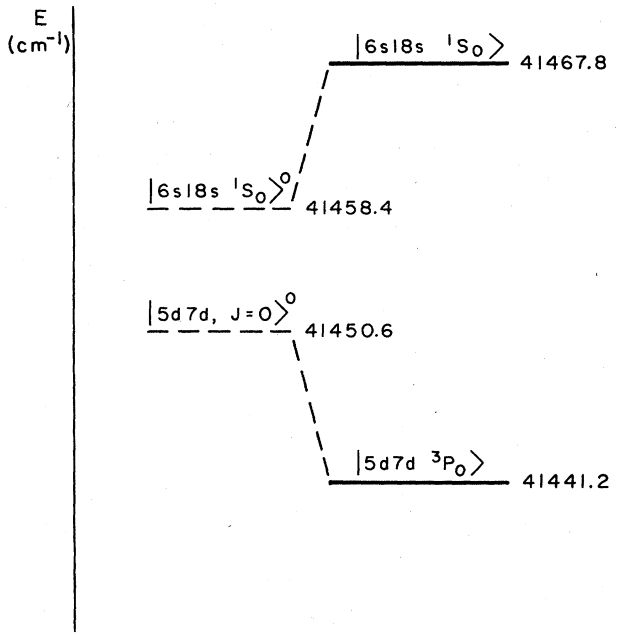

FIG. 5. Real (——) and pure-configuration (— — —) states used to determine the absolute value of the electrostatic quadrupole matrix element mixing the $|6s18s\,^1S_0\rangle^0$ and $|5d7d, J=0\rangle^0$ states.

obtained in the MQDT analysis of Aymar *et al.*[11] Owing to the symmetry of the two-level model the admixture coefficient $Z_2^2(18)$ should have the same value of 0.35 which is somewhat higher than the value of 0.28 (Table I). The value of $Z_2^2(18)=0.35$ is approached only if all Z_2^2 of the neighboring $6sns$ levels are summed. This indicates the extent to which the two-level treatment is valid, and it also predicts the absolute value of the configuration interaction matrix element $|\langle V\rangle|$. If the sign of $\langle V\rangle$ could be predicted theoretically, the signs of the Z_2 would also be fixed. The calculation is further complicated because the $|5d7d,J=0\rangle$ state is neither a pure $^1S_0$ nor $^3P_0$ state, owing to strong spin-orbit coupling.[11] In this respect, a three-channel model [Eq. (3)] would have been preferable but the data did not allow a fit with a larger number of adjustable ionization amplitudes.

VII. CONCLUSION

The analysis of the photoionization data has led to a set of relative signs for the admixture coefficients Z_1 and Z_2 of the intermediate Rydberg levels and to ionization amplitudes, reproducing the angular distribution data. The most startling features observed experimentally were the low line intensity in the spectra when exciting via the $6s18s\,^1S_0$ state and the fact that the most isotropic angular distribution was found for the $6s18s\,^1S_0$ state and not for the $5d7d\,^3P_0$ doubly excited state. The ultimate reason for both effects was found to be a change in the

sign of Z_2 when going from the $5d7d\,^3P_0$ to the $6s\,18s\,^1S_0$ state. This sign change is only another manifestation of the localized nature of the $5d\,7d$-$6sns$ interaction. Based on this fact the magnitude of the electrostatic quadrupole interaction matrix element has been determined using a simple theoretical model. The amplitude and relative phase of the ionizing transition have also been extracted from the data. By far the largest amplitude was found for the transition from the $5d\,7d$, $J=0$ pure configuration state to the $6s_{1/2}$, $\epsilon p_{1/2}$ partial wave indicating strong channel mixing between $J=1$ states extending into the continuum. Finally, it has been rather satisfying to find that the set of $Z_1(n)$ and $Z_2(n)$ could be used to calculate relative absorption line strengths that match the experimental observations surprisingly well.

ACKNOWLEDGMENTS

We are grateful to K. T. Lu for drawing our attention to this problem. It is a pleasure to acknowledge numerous fruitful discussions with A. R. P. Rau and M. Aymar, and the help of C. V. Kunasz with the data analysis. This work was financially supported by the Deutsche Forschungsgemeinschaft and by the National Science Foundation through Grant No. PHY-82-00805 to the University of Colorado.

*Quantum Physics Division, National Bureau of Standards.

[1]U. Fano, Rep. Prog. Phys. **46**, 97 (1983).
[2]M. J. Seaton, Rep. Prog. Phys. **46**, 167 (1983).
[3]M. Aymar, Phys. Rep., **110**, 163 (1984); for Ba, see also, J. Opt. Soc. Am. B **1**, 239 (1984).
[4]M. Aymar, P. Grafström, C. Levison, H. Lundberg, and S. Svanberg, J. Phys. B **15**, 877 (1982).
[5]R. D. Hudson, V. L. Carter, and P. A. Young, Phys. Rev. A **2**, 643 (1970).
[6]P. Lambropoulos, Adv. At. Mol. Phys. **12**, 87 (1976).
[7]G. Leuchs and H. Walther, in *Multiphoton Ionization of Atoms,* edited by S. L. Chin and P. Lambropoulos (Academic, Toronto, Orlando, and London, 1984), p. 109.
[8]E. Matthias, P. Zoller, D. S. Elliott, N. D. Piltch, S. J. Smith, and G. Leuchs, Phys. Rev. Lett. **50**, 1914 (1983).
[9]G. Leuchs, in *Laser Physics,* Vol. 182 of *Lecture Notes in Physics,* edited by J. D. Harvey and D. F. Walls (Springer, Berlin, Heidelberg, New York, and Tokyo, 1983), p. 174.
[10]R. J. Fonck, F. L. Roesler, D. H. Tracy, K. T. Lu, F. S. Tomkins, and W. R. S. Garton, Phys. Rev. Lett. **39**, 1513 (1977).
[11]M. Aymar, P. Camus, M. Dieulin, and C. Morillon, Phys. Rev. A **18**, 2173 (1978).
[12]J. Neukammer, E. Matthias, and H. Rinneberg, Phys. Rev. A **25**, 2426 (1982).
[13]U. Fano, Phys. Rev. **124**, 1866 (1961).
[14]A. F. Starace, in *Handbuch der Physik,* edited by W. Mehlhorn, (Springer, Berlin, 1982), p. 1.
[15]K. T. Lu and A. R. P. Rau, Phys. Rev. A **28**, 2623 (1983).
[16]J. A. Armstrong, J. J. Wynne, and P. Esherick, J. Opt. Soc. Am. **69**, 211 (1979).
[17]K.-N. Huang and A. F. Starace, Phys. Rev. A **19**, 2335 (1979).
[18]H. Rinneberg, J. Neukammer, and E. Matthias, Z. Phys. A **306**, 11 (1982).
[19]U. Fano and J. W. Cooper, Rev. Mod. Phys. **40**, 441 (1968).
[20]U. Fano, Phys. Rev. **178**, 131 (1969).
[21]J. A. R. Sampson, in *Handbuch der Physik,* edited by W. Mehlhorn (Springer, Berlin, 1982), p. 184.
[22]J. R. Rubbmark, S. A. Borgström, and K. Bockasten, J. Phys. B **10**, 421 (1977).
[23]J. Kelly (private communication).
[24]C.-M. Lee and K. T. Lu, Phys. Rev. A **8**, 1241 (1973), see Eq. (2.11).
[25]D. L. Moores and H. E. Saraph, in *Atoms in Astrophysics,* edited by P. G. Burke, W. B. Eissner, D. G. Hummer, and I. C. Percival (Plenum, New York and London, 1983), p. 173.
[26]G. Peach, Mem. R. Astron. Soc. **71**, 13 (1967).